

Influence of High CO₂ Partial Pressure on Top-of-the-Line Corrosion

Maryam Eslami
Institute for Corrosion and Multiphase
Technology, Ohio University
342 West State St.
Athens, Ohio 45701
United States

Maria Eduarda Dias Serenário
Institute for Corrosion and Multiphase
Technology, Ohio University
342 West State St.
Athens, Ohio 45701
United States

Bernardo Augusto Farah Santos
Institute for Corrosion and Multiphase
Technology, Ohio University
342 West State St.
Athens, Ohio 45701
United States

Sondre Gjertsen
Institute for Energy Technology &
University of Stavanger
Kjeller
Norway

David Young
Institute for Corrosion and Multiphase
Technology, Ohio University
342 West State St.
Athens, Ohio 45701
United States

Marc Singer
Institute for Corrosion and Multiphase
Technology, Ohio University
342 West State St.
Athens, Ohio 45701
United States

ABSTRACT

Top-of-the-line corrosion (TLC) is an important type of material degradation that occurs due to the heat exchange between the pipeline and its surroundings, which results in water condensation on the internal surface of the pipe. This type of corrosion is specific to wet gas pipelines with stratified flow regimes. In this research, the effect of high CO₂ partial pressure (pCO₂) on TLC rate and mechanism was studied. The experiments were conducted in a high-pressure TLC autoclave with pCO₂ ranging from 20 to 100 bar, solution temperatures of 30 and 50 °C, and different water condensation conditions (0.001-0.1 ml/m².s). The experimental conditions covered environments where CO₂ was either gaseous or supercritical. The results revealed that uniform and localized TLC rates increase with water condensation rate and solution temperature. However, as long as CO₂ remained gaseous, pCO₂ showed a negligible influence on both uniform and localized TLC rates. At a high CO₂ content, the formation of a protective FeCO₃ layer decreased the TLC rate, especially at lower water condensation rates. Nevertheless, the risk of localized corrosion at high and medium water condensation rates remained an issue. In the supercritical CO₂ environment (pCO₂ of 100 bar and solution temperature of 50 °C), the difference in temperature between the CO₂ dense phase and the specimens caused water drop out and corrosion. In this environment, the high pCO₂ and low pH of the dropped-out water led to high uniform and localized

corrosion rates. However, under this condition, the difference in corrosion rates of specimens with different cooling rates was negligible due to their similar surface temperature.

Keywords: Sweet corrosion, Top-of-the-line corrosion, Localized Corrosion, Supercritical CO₂

INTRODUCTION

Pipeline corrosion during the transportation of fluids is a well-known problem in the oil and gas industry. The unprocessed fluid extracted from an oil well is typically a complex mixture of oil, solids, gas, and brine (water phase). The presence of water, in which the corrosive gases (CO₂, H₂S) can dissolve and produce weak acids, results in corrosion. In the 1990s, a new mode of corrosion was identified which today is known as top-of-the-line corrosion or TLC. TLC is observed in wet gas transport pipelines at the upper part of the pipe (with a stratified flow regime), where the pipe is not directly in contact with the water phase. TLC of course occurs when the gas contains condensable liquids, e.g., water and some hydrocarbons. The prerequisite for TLC is the heat exchange between the pipeline and its colder surroundings.^{1, 2} This heat exchange leads to the condensation of water or hydrocarbon phases on the cold walls of the pipelines, as a thin film or in droplets. The condensed water phase that contains CO₂, H₂S, and organic acids such as acetic acid can be, at least initially, very corrosive to carbon steel pipelines causing loss of integrity and eventually failure.³⁻⁷

As defined above, TLC is a complicated phenomenon depending on the factors affecting the heat and mass transfer, including temperature gradient across the pipe wall, gas temperature and flow rate, as well as chemistry of the condensed water, such as the acidic gas and organic acid content. Considering sweet corrosion scenarios where the main corrosive species is CO₂, the partial pressure of CO₂ together with the temperature gradient between the gas phase and the pipeline surface are two of the main factors to be studied for the TLC rate estimation. A few parametric studies are available on the effect of these two parameters on TLC.^{4, 8-13} The studies on the effect of temperature (mostly T_g (gas temperature) and T_s (surface temperature)), or the condensation rate (as the one variable directly affected by the temperature) have naturally focused on the formation of protective corrosion product layers (i.e., iron carbonate, FeCO₃) and how it affects the TLC rate and mechanism. The available studies cover a wide range of water condensation rates from 0.001 ml/m².s to 2 ml/m².s⁸ and they also include water/hydrocarbon co-condensation scenarios.^{14, 15}

On the other hand, the range of CO₂ partial pressures that is covered in the literature available to this date usually does not exceed 10 bar.¹³ Considering the inevitable influence of CO₂ partial pressure on the formation of FeCO₃ and the necessity of moving toward systems with higher pressure, especially with the demand for CO₂ storage and capture purposes, it is essential to study TLC under conditions with high CO₂ pressure.

In the current paper, a parametric study is described relating to the influence of temperature and CO₂ partial pressure on TLC of carbon steel with an emphasis on high CO₂ pressure (up to 100 bar), employing weight loss corrosion measurements and surface characterization techniques such as scanning electron microscopy (SEM), Raman spectroscopy, and optical profilometry.

EXPERIMENTAL PROCEDURE

TLC setup and testing procedure

A 20 L autoclave made of alloy C-276 (UNS N10276), designed to simulate TLC scenarios, was used to conduct the experiments. The TLC experiments were performed at three different water condensation rates named as “High-water condensation rate (HWCR)”, “Low-water condensation rate (LWCR)”, and “(in) Gas phase” condition. Figure 1 depicts the specimen configuration within the autoclave along with simulation-derived water condensation rate values for the experimental conditions of this study. Six X65 steel¹⁶ specimens were placed in the TLC corrosion specimen holder which was then screwed to the

autoclave lid. This holder is in contact with a coiled tubing chiller system inside the lid that cools down the sample holder and the specimens. The chiller system is run by using a chilled glycol solution that is circulated in the system from an external source. This external source is equipped with a pump and a temperature control/monitoring system. In this study, the water condensation rate on each specimen was controlled by adjusting the temperature difference between the gas phase and the surface of the specimen. At a fixed condition, the higher the temperature difference, the higher the water condensation rate would be. As shown in Figure 1, the specimens that are directly flush mounted to the holder are under high(er) water condensation rate condition (HWCR) as they are directly in contact with the chiller system and therefore have a greater temperature difference with the gas phase. The specimens that are placed in the PEEK holders are at low(er) water condensation rate condition (LWCR) as they are separated from the chiller system with a layer of PEEK with low thermal conductivity and therefore are at a higher temperature and have a smaller temperature difference with the gas phase. The specimens that are separated from the chiller system with a stud (as shown in Figure 1) are named (in) Gas phase specimens and have the lowest water condensation rate. In all cases, the actual value of WCR is always quite low (<0.1 mL/m²/s). The “HWCR”, “LWCR” and “Gas Phase” are used for ease of comprehension.

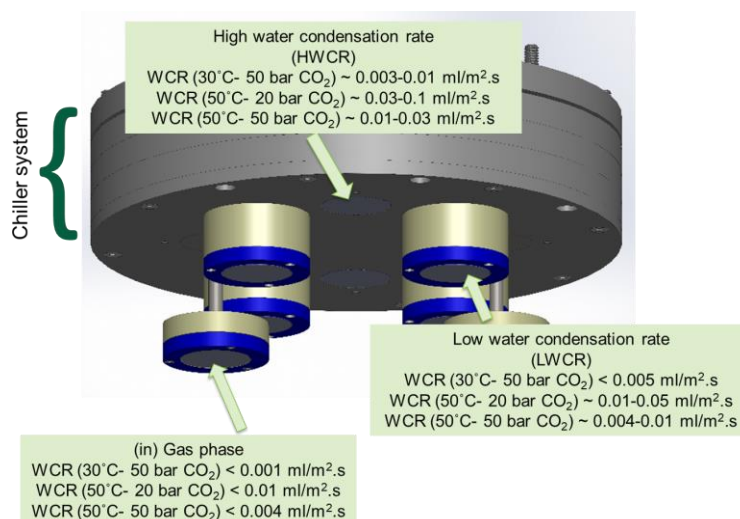


Figure 1: The internal autoclave lid TLC specimen setup.

**Table 1
Experimental conditions for the TLC experiments**

Test ID	Solution temperature (°C)	CO ₂ partial pressure (bar)	Duration (days)
1-1	30	50	2
1-2	30	50	7
1-3	30	50	21
2	50	20	21
3	50	50	21
4 (Supercritical CO ₂)	50	100	21

The experimental conditions of this study are outlined in Table 1. The first three experiments (1-1 to 1-3) were performed to determine the optimal testing duration, in terms of detection of localized corrosion. The duration of the next three experiments was selected based on the results of these first three experiments.

It should be noted that under the conditions of experiment 4, CO₂ will turn into a supercritical phase. Therefore, water condensation does not occur as it only occurs in a gas/liquid system. Instead, a similar phenomenon known as water drop-out happens. The solubility of water in CO₂ depends not only on its

pressure but also on the temperature.¹⁷ The change in temperature of the CO₂ dense phase, as it approaches the chilled sample holder, causes a change in its water solubility and therefore water drop-out. Similar to the condensed water, this water is corrosive to the steel specimen due to the presence of dissolved CO₂. Accordingly, the names of specimens for experiment 4 are changed to HWDR, LWDR, and Dense Phase.

The following experimental procedure was pursued. Before each experiment, the autoclave body was cleaned with isopropanol and deionized (DI) water, followed by wiping with a paper towel. 12 liters of DI water was then poured into the autoclave and sparged with CO₂ for at least 12 hours for deoxygenation. The temperature of the solution was simultaneously increased to the target temperature. Six weight loss specimens of X65 steel (two for HWCR, two for LWCR, and two for Gas phase conditions) were sequentially polished up to 600 grit using SiC abrasive papers. After polishing, the specimens were ultrasonically cleaned with isopropanol and air dried, and the initial mass of each specimen was measured using a balance of 0.1 mg precision. After the desired solution temperature was reached, the system was opened, and the specimens were placed in the top lid. As mentioned earlier, the autoclave lid is equipped with an internal cooling system connected to an external source. The temperature of the glycol solution in the external source was accordingly set to have a temperature difference of 10 °C between the HWCR specimens and the gas phase. After closing the autoclave, any remaining oxygen in the brine, headspace, and lines was purged with CO₂. An oxygen sensor was connected to the pressure release valve and the oxygen concentration for all the tests did not exceed 5 ppb. After checking the oxygen concentration, the autoclave was pressurized to the target CO₂ pressure and then heated to the desired temperature. The temperature of the gas, the solution, and the HWCR steel specimens were monitored during the experiment.

Post-processing methodology

After the experiments, according to ASTM Standard G1-03,¹⁸ the corrosion products on the corroded specimens were removed using Clarke solution. Specimens were then rinsed with DI water and isopropanol and subsequently air dried. The corrosion rate was calculated using the difference between the initial and the final weight of each specimen before and after the cleaning process. The following equation was used:

$$CR = 87600\Delta m/\rho At \quad (1)$$

where CR is the corrosion rate in mm/y, Δm is the mass difference in grams, ρ is the density of carbon steel (7.874 g/cm³), A is the exposed area in cm², and t is time in hours.

After the corrosion tests (and before Clarke solution cleaning), the surfaces of the specimens were examined using scanning electron microscopy (SEM), energy dispersive X-ray spectroscopy (EDS), Raman spectroscopy, and optical profilometry.

Apart from the corrosion rate obtained from the weight loss measurements, the maximum penetration rate for each specimen was determined from the optical profilometry data using determined maximum penetration depth and a simple proportion calculation.

RESULTS

The effect of test duration

In the first part of this research, the effect of test duration on uniform TLC rate and the occurrence of localized corrosion at three different water condensation conditions was investigated. These series of experiments were done at a solution temperature of 30 °C and pCO₂ of 50 bar; experimental durations of 2, 7, and 21 days were selected.

Figure 2 depicts the results for TLC rate as a function of test duration for HWCR, LWCR, and Gas phase specimens. Firstly, as shown in this figure, regardless of the test duration, the uniform TLC rate (calculated based on weight loss measurements) increases with the water condensation rate. This trend can be explained by the possible formation of protective corrosion product layers.¹⁹ At a high water condensation rate, such as the condition of HWCR specimen, the refreshment of condensed water droplets on the specimen dilutes the existing water film and limits or decreases the saturation value with regard to FeCO_3 ($S_{\text{FeCO}_3} = [\text{Fe}^{2+}][\text{CO}_3^{2-}]/K_{\text{sp,FeCO}_3}$). This disrupts the formation of a protective FeCO_3 layer or leads to the dissolution of any formed layer. However, in LWCR and Gas phase conditions, the refreshment of condensed water on the surface of the specimen is slower due to the lower condensation rates and longer droplet retention time,⁸ therefore, the FeCO_3 layer can form and decrease the corrosion rate.

Regarding the test duration, according to Figure 2, it seems that the rate of uniform TLC decreases with time, and this is independent of the water condensation rate.

To understand the effect of time and condensation rate on the formation of corrosion product layers and the occurrence of localized corrosion, the specimen surfaces after the 2-day, 7-day, and 21-day experiments were further characterized.

Figure 3 shows the SEM images of surfaces of the specimens after 2 days of the experiment. The images in this figure were taken at two different magnifications, providing a representative view of the entire surface at a lower magnification (50x) and the detailed morphology of the corrosion products at a higher magnification (2000x). As was hypothesized earlier, the surface of the specimen at HWCR condition is only partially covered by the corrosion products (possibly FeCO_3). This is obvious by looking at the high magnification image where the crystals of corrosion products are seen on top of a corroded matrix. On the other hand, the surfaces of the specimens in LWCR and Gas phase conditions are entirely covered by a dense, and hence protective, layer of corrosion product. The composition of the corrosion product layers on the three specimens was investigated by EDS (the results are not shown here). The EDS results are not conclusive and cannot be used to identify phases, however, due to the presence of Fe, O, and C they suggest that the corrosion product is most probably FeCO_3 .

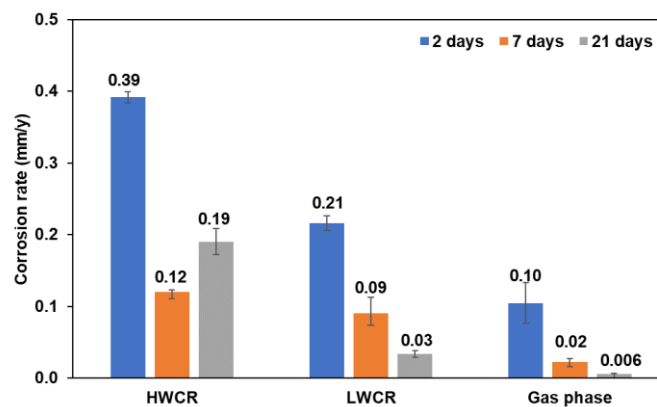


Figure 2: Results of corrosion rate after TLC experiment under different water condensation rates at T_{sol} of 30 °C with $p\text{CO}_2$ of 50 bar for 2, 7, and 21 days (the error bars show max and min).

The occurrence of localized corrosion during TLC is one of the most important subjects from both industrial and research standpoints. Therefore, after removing the corrosion product layers, the surfaces of the three specimens were characterized by optical profilometry to investigate the presence of such corrosion features. The results are shown in Figure 4. According to this figure, no sign of localized corrosion on any of the specimens was observed after 2 days of experiment. The results of SEM, EDS, and optical profilometry of the specimens after the 7-day experiment were identical to those after the 2-

day experiment. In this case also, no sign of localized corrosion was observed on the specimens. Therefore, to avoid repetition, the results are not presented here.

The SEM images of the surface of specimens after the 21-day experiment are shown in Figure 5. According to the figure, compared to the 2-day experiment (Figure 3), the HWCR specimen is entirely covered by a layer of corrosion product. The LWCR and Gas phase specimens are also covered by seemingly dense corrosion product layers. The composition of the corrosion product layer on each of these specimens was characterized using Raman spectroscopy and the results are shown in Figure 6. According to the Raman data, the corrosion product formed under each condensation condition is FeCO_3 .²⁰

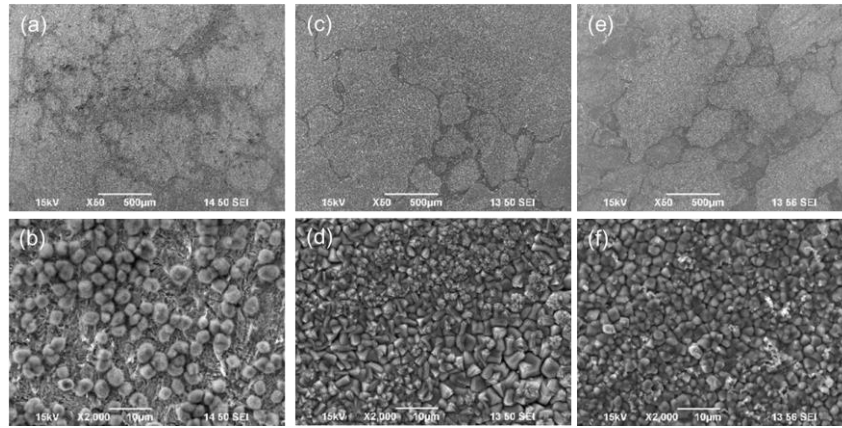


Figure 3: SEM analysis of corrosion product after the TLC experiment under different water condensation rates at T_{sol} of 30 °C with $p\text{CO}_2$ of 50 bar for 2 days: (a) and (b) HWCR; (c) and (d) LWCR; (e) and (f) Gas phase.

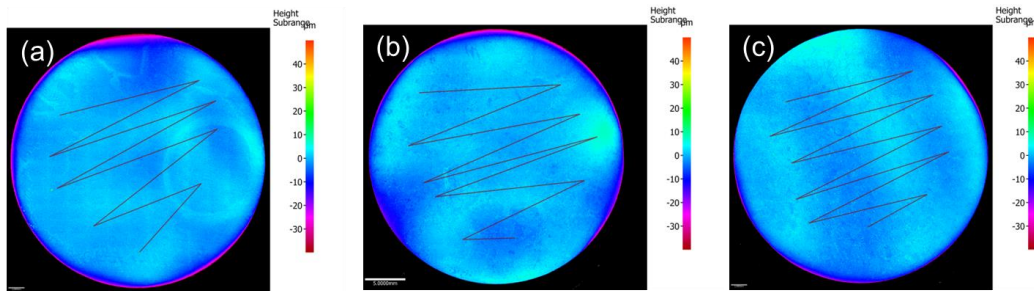


Figure 4: Optical profilometry analysis of the surface of specimen after the TLC experiment under different water condensation rates at T_{sol} of 30 °C with $p\text{CO}_2$ of 50 bar for 2 days: (a) HWCR; (b) LWCR; (c) Gas phase.

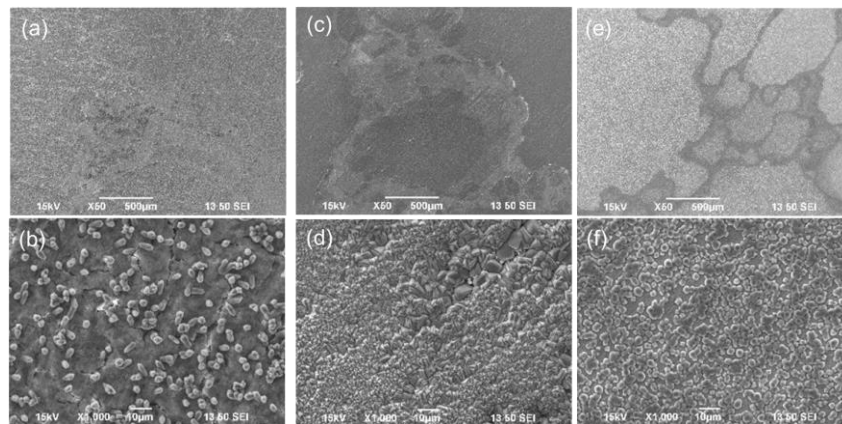


Figure 5: SEM analysis of corrosion product after the TLC experiment under different water condensation rates at T_{sol} of 30 °C with $p\text{CO}_2$ of 50 bar for 21 days: (a) and (b) HWCR; (c) and (d) LWCR; (e) and (f) Gas phase.

The presence of localized corrosion features at three different water condensation conditions after the 21-day experiment was investigated using optical profilometry and the results are shown in Figure 7. According to these figures, after 21 days of experiment, localized corrosion features appear on HWCR and LWCR specimens. These localized features are larger in size on the HWCR specimen and slightly deeper on the LWCR specimen. This difference can be related to the water condensation rate, where on the HWCR specimen larger areas of the FeCO_3 layer are compromised due to the higher water condensation rate and a faster refreshment of the existing liquid film with new hence unsaturated condensed water with respect to FeCO_3 . On the LWCR specimen, smaller areas of the protective FeCO_3 are damaged, however, the corrosion is deeper at those sites. No localized corrosion on the Gas phase specimen was found.

The results of this part showed that the TLC at three different condensation conditions was uniform during the first 7 days of the experiment and the specimens exposed to high and low water condensation rates showed localized corrosion features after 21 days. According to these results, the duration of 21 days was selected for the next experiments of this study.

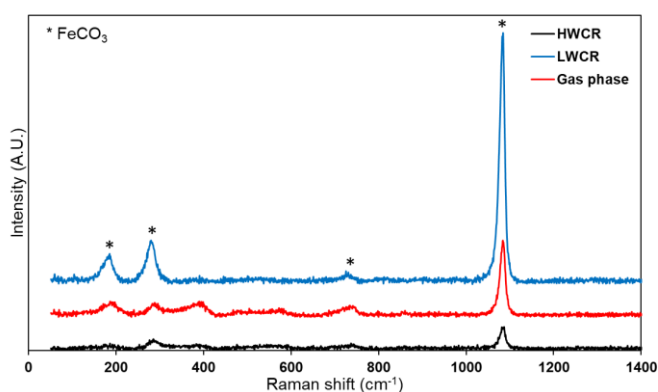


Figure 6: Raman spectra of corrosion products after the TLC experiment under different water condensation rates at T_{sol} of 30 °C with $p\text{CO}_2$ of 50 bar for 21 days.

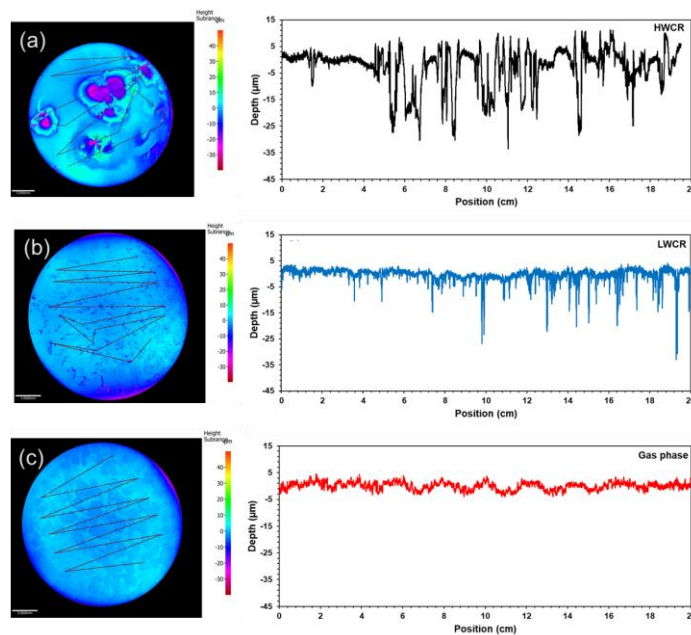


Figure 7: Optical profilometry analysis of the surface of specimen after the TLC experiment under different water condensation rates at T_{sol} of 30 °C with $p\text{CO}_2$ of 50 bar for 21 days: (a) HWCR, (b) LWCR, and (c) Gas phase.

The effect of $p\text{CO}_2$

The results of uniform TLC rate as a function of $p\text{CO}_2$ for the three water condensation conditions are shown in Figure 8. It should be mentioned that the results of the experiment under 100 bars of CO_2 , which corresponds to supercritical CO_2 condition, are discussed later in this manuscript. According to Figure 8, at LWCR and Gas phase conditions, the uniform TLC rate decreases with the increase in $p\text{CO}_2$ from 20 to 50 bar. This decrease can be linked to the formation of a protective FeCO_3 layer that decreases the corrosion rate and is more favored at a higher $p\text{CO}_2$, due to the higher concentration of $[\text{CO}_3^{2-}]$ and therefore a higher supersaturation value. The same decrease in corrosion rate cannot occur under HWCR condition, as evidenced in Figure 8. This is mainly due to the higher water condensation rate²¹, faster rate of water refreshment and lower droplet retention time⁸ that impede the formation of a protective FeCO_3 layer.

The aforementioned discussion regarding the formation of FeCO_3 and its relationship with the water condensation rate and $p\text{CO}_2$ was further investigated by analyzing the surfaces of the specimens, using SEM and Raman spectroscopy. The SEM images of the surfaces of the specimens after the experiment at $p\text{CO}_2$ of 20 bar (in Figure 9), together with the results of Raman spectroscopy analysis (Figure 10), show the formation of a FeCO_3 layer at LWCR and Gas phase conditions. According to Figure 9, at these two conditions, the surface is entirely covered by FeCO_3 crystals that form a dense and protective layer. At HWCR condition, the surface of the specimen is only partially covered by small crystals of (supposedly) FeCO_3 which are not effective in decreasing the corrosion rate. The results of Raman spectroscopy analysis on the HWCR specimen did not show the presence of any FeCO_3 , hence it is not shown here. This could be due to the low amount of FeCO_3 present on the surface of this specimen.

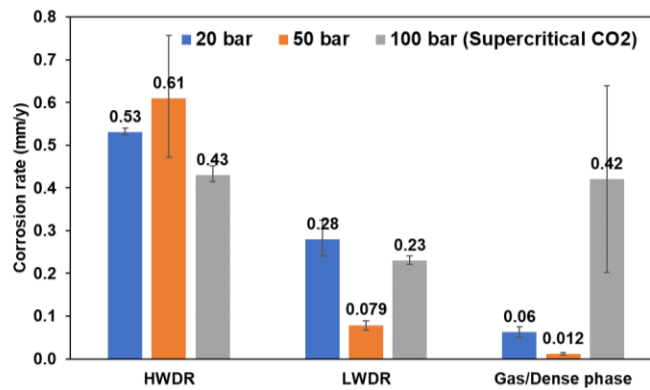


Figure 8: Results of corrosion rate after TLC experiment under different condensation rates after 21 days at T_{sol} of 50 °C with $p\text{CO}_2$ of 20 bar, 50 bar, and 100 bar (the error bars show max and min).

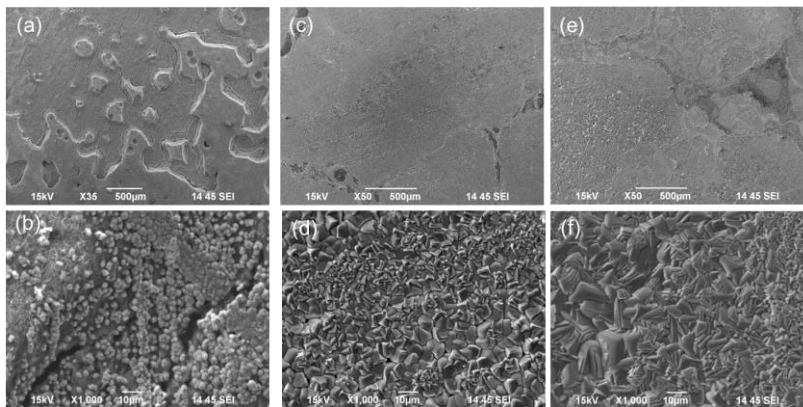


Figure 9: SEM analysis of corrosion product after the TLC experiment under different water condensation rates at T_{sol} of 50 °C with $p\text{CO}_2$ of 20 bar for 21 days: (a) and (b) HWCR; (c) and (d) LWCR; (e) and (f) Gas phase.

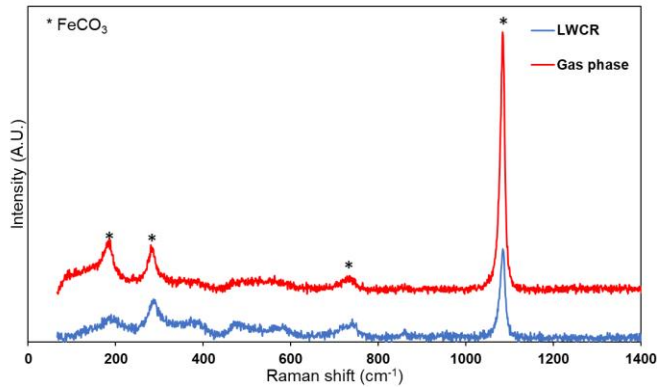


Figure 10: Raman spectra of corrosion products after the TLC experiment under different water condensation rates for T_{sol} 50 °C with $p\text{CO}_2$ of 20 bar for 21 days.

At $p\text{CO}_2$ of 50 bar, the results of SEM and Raman spectroscopy (shown in Figure 11 and Figure 12) at LWCR and Gas phase conditions are similar to those at $p\text{CO}_2$ of 20 bar. Interestingly, at $p\text{CO}_2$ of 50 bar, the surface of the HWCR specimen is also covered by FeCO_3 crystals, however, as evidenced by the TLC rate in Figure 8, this FeCO_3 layer is not protective and does not decrease the corrosion rate. After removing the corrosion products, the surfaces of specimens from these two experiments (at $p\text{CO}_2$ of 20 and 50 bar) were analyzed using optical profilometry to investigate the presence of localized corrosion features. The results are shown in Figure 13 and Figure 14.

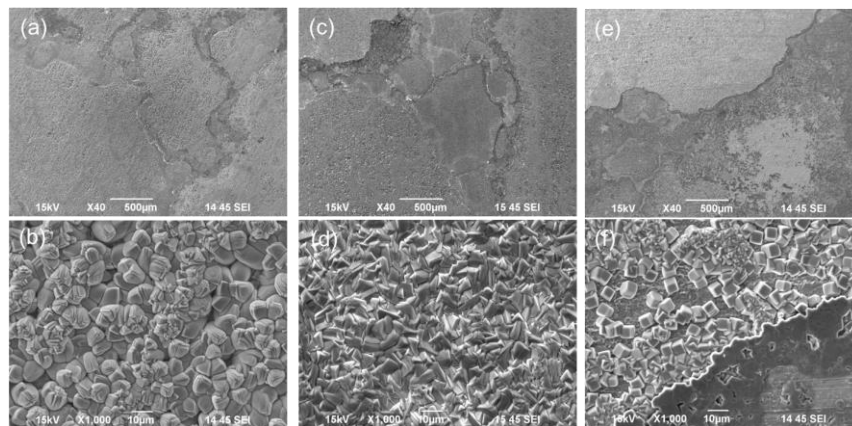


Figure 11: SEM analysis of corrosion product after the TLC experiment under different water condensation rates for T_{sol} : 50 °C with $p\text{CO}_2$ of 50 bar for 21 days: (a) and (b) HWCR; (c) and (d) LWCR; (e) and (f) Gas phase.

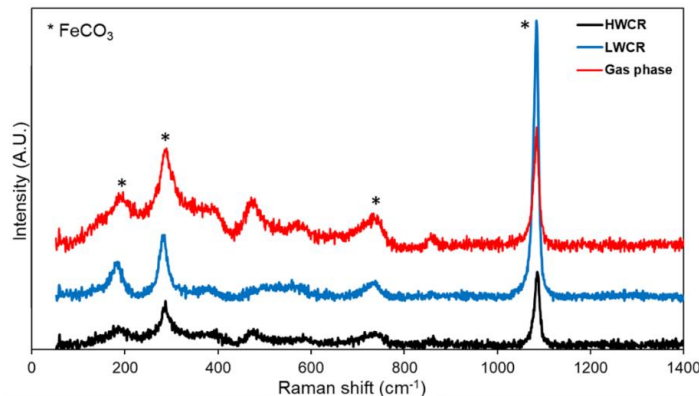


Figure 12: Raman spectra of corrosion products after the TLC experiment under different condensation rates at T_{sol} of 50 °C with $p\text{CO}_2$ of 50 bar for 21 days.

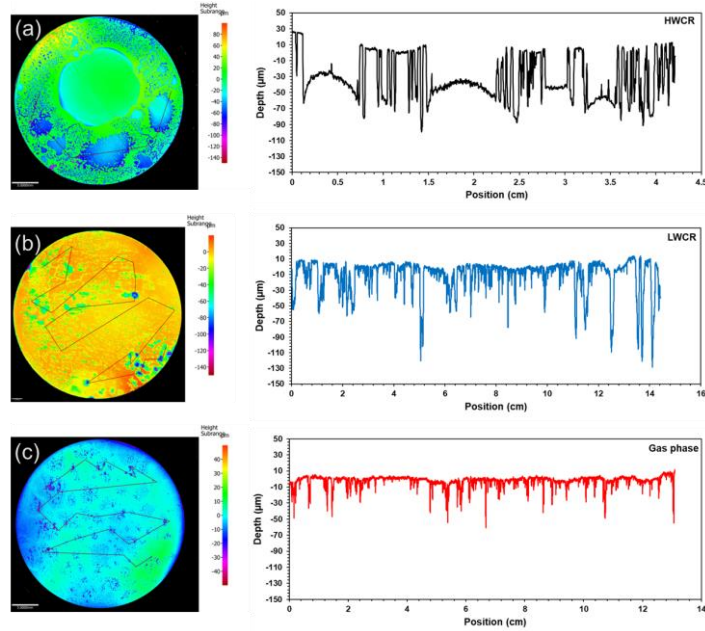


Figure 13: Optical profilometry analysis of the surface of specimen after the TLC experiment under different condensation conditions at T_{sol} of 50 °C with pCO_2 of 20 bar for 21 days: (a) HWCR, (b) LWCR, and (c) Gas phase.

For HWCR condition at pCO_2 of 20 and 50 bar, the localized corrosion features are relatively large with an average depth of approximately 80 μm . At pCO_2 of 20 bar and in LWCR condition, the localized corrosion features are smaller in size, however, they are deeper when compared to the HWCR condition at the same pCO_2 . Interestingly, according to Figure 14, at LWCR condition, the depth of localized corrosion features seemingly decreases with pCO_2 . A similar observation is noted for the Gas phase condition. At pCO_2 of 20 bar, under the Gas phase condition, the localized corrosion features are smaller in size and less deep compared to LWCR and HWCR conditions. At pCO_2 of 50 bar for Gas phase condition no localized corrosion was observed.

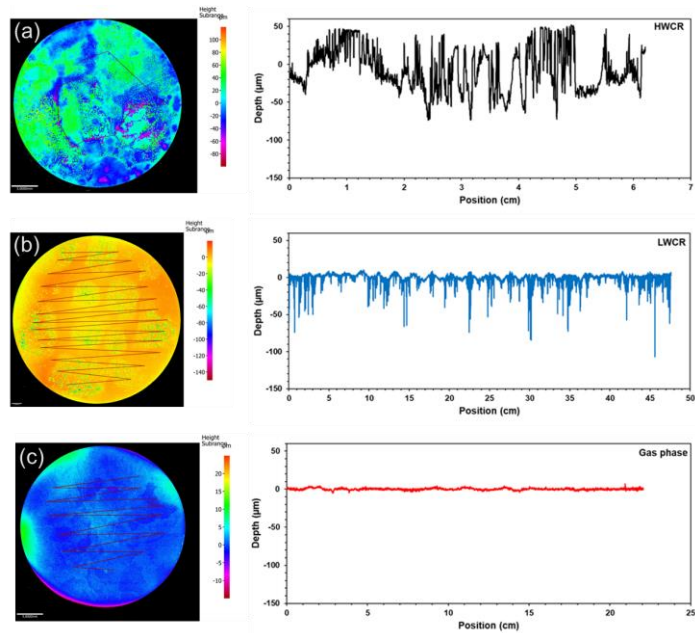


Figure 14: Optical profilometry analysis of the surface of specimen after the TLC experiment under different condensation conditions at T_{sol} of 50 °C with pCO_2 of 50 bar for 21 days: (a) HWCR, (b) LWCR, and (c) Gas phase.

The effect of supercritical CO₂ condition

The results of the experiment under supercritical CO₂ condition are discussed in this part. According to Figure 8, the corrosion rates at three different water drop-out conditions are similar. These results can be related to the fact that, despite our efforts, the water drop-out rates were similar for all specimens. Figure 15 depicts the variation of temperature for the dense CO₂ phase, the solution at the bottom of the autoclave, and the cooled surface of the HWDR specimen during the experiment.

As can be observed in this graph, the temperature difference between the dense CO₂ and the HWDR specimen (that is supposedly the coldest specimen) is minimal. In the earlier experiments, all specimens were located in the gas phase, however, in this experiment, the specimens are located in the dense CO₂ phase. The increase in heat capacity from the CO₂ gas phase to the CO₂ supercritical phase²² makes cooling the specimens exposed to the supercritical dense phase quite difficult. Therefore, it can be concluded that during this experiment all specimens were in similar water drop-out conditions.

The surfaces of the specimens were further analyzed with regard to the corrosion product layers and the presence of localized corrosion. As shown in the SEM images in Figure 16, all three specimens (HWDR, LWDR, and Dense phase) are covered by crystals of FeCO₃ (as proved by the Raman data in Figure 17). The surfaces of the specimens were further analyzed after removing the corrosion products in terms of localized corrosion. The results of optical profilometry in Figure 18 show that all specimens suffered from localized corrosion in a depth range of 200-250 μm, which was significantly deeper than those observed in the previous experiments. This is because the low pH (due to high CO₂ content)¹⁷ under the conditions of this experiment makes the environment significantly corrosive.

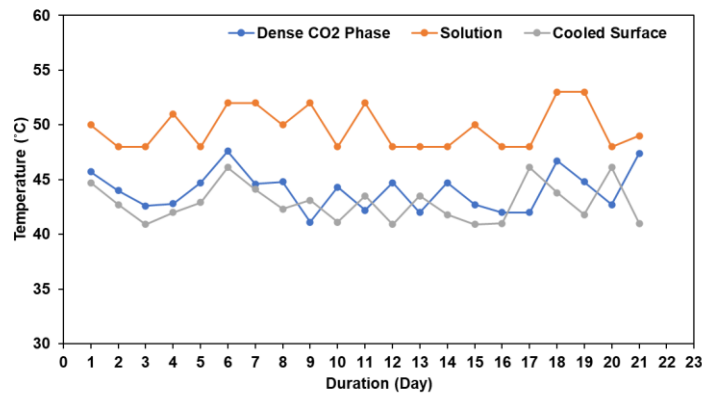


Figure 15: The variation of temperature for dense CO₂ phase, solution, and cooled surface (HWDR specimen) during the experiment at T_{sol} of 50 °C with pCO₂ of 100 bar for 21 days.

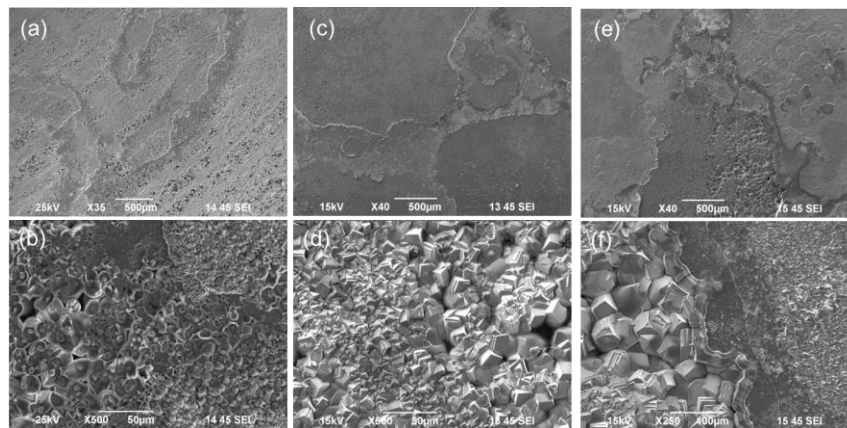


Figure 16: SEM analysis of corrosion product after the experiment under different water drop-out rates at T_{sol} of 50 °C with pCO₂ of 100 bar for 21 days: (a) and (b) HWDR; (c) and (d) LWDR; (e) and (f) Dense phase.

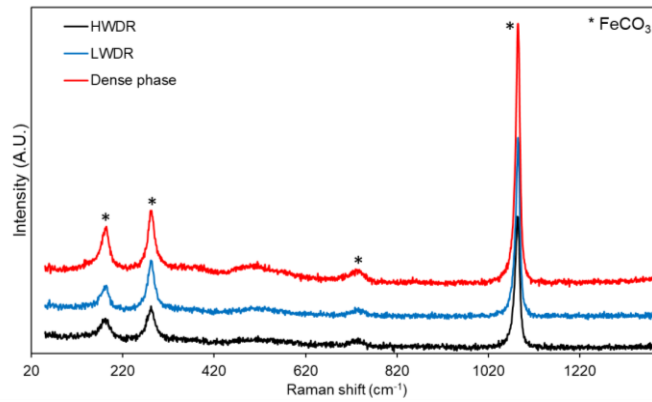


Figure 17: Raman spectra of corrosion products after the experiment under different water drop-out conditions at T_{sol} of 50 °C with pCO_2 of 100 bar for 21 days.

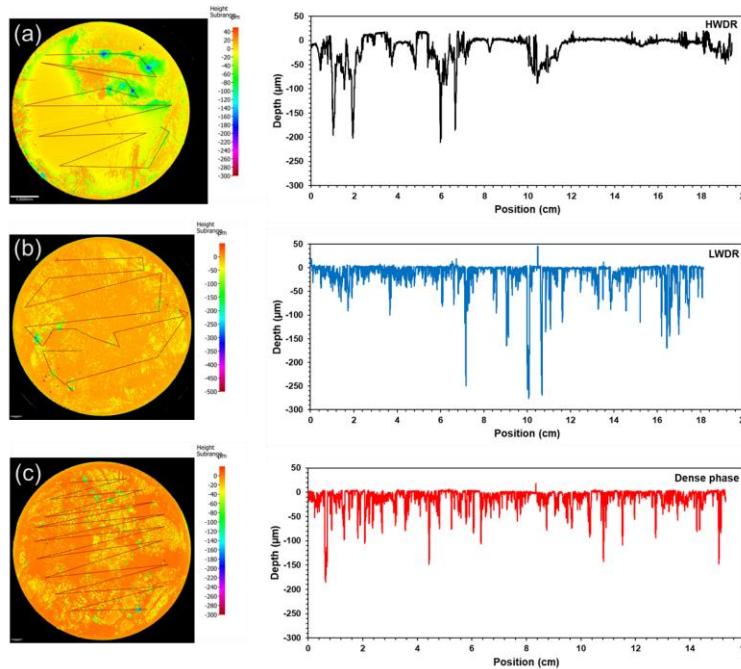


Figure 18. Optical profilometry analysis of the surface of specimen after the experiment under different water drop-out conditions for T_{sol} 50 °C with pCO_2 100 bar for 21 days: (a) HWDR; (b) LWDR; and (c) Dense phase.

Discussion

Figure 19 shows the results of uniform TLC and maximum penetration rate as a function of surface temperature for the specimens after the TLC experiment at pCO_2 of 50 bar, and solution temperature of 30 °C and 50 °C. As explained earlier in this manuscript, during each experiment, the specimens were under three different water condensation rates. According to Figure 19 (a), the corrosion rate at LWCR and Gas phase conditions seems independent of the surface temperature, however, it increases with the surface temperature at HWCR condition. Since at LWCR and Gas phase conditions the surface is protected by $FeCO_3$, the change in surface temperature does not affect the TLC rate. At HWCR condition, at both surface temperatures, the metal surface is not protected by the corrosion product layer and is exposed to further corrosion. In this case, the increase in corrosion rate with temperature could be simply related to the increased kinetics of the electrochemical reactions by the increase in temperature.²³

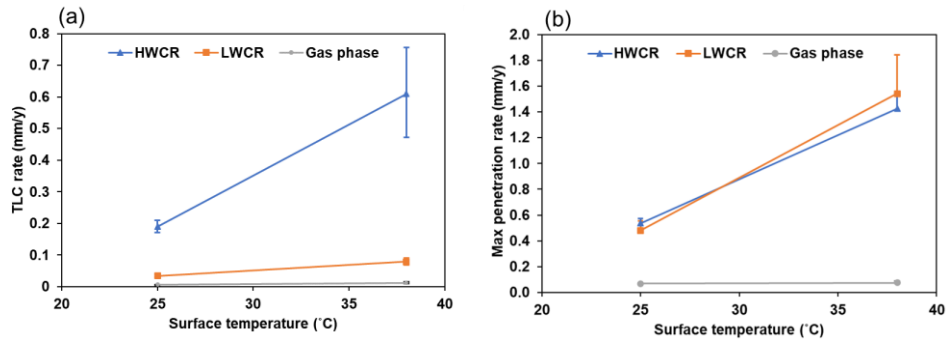


Figure 19: (a) uniform TLC and (b) maximum penetration rate as a function of steel surface temperature and condensation rate ($p\text{CO}_2$ of 50 bar, duration of 21 days, error bars show max and min).

According to the results of the maximum penetration rate as a function of surface temperature in Figure 19 (b), the risk of localized corrosion exists at HWCR and LWCR conditions, and the maximum penetration rate increases with the surface temperature. This means that for both conditions of high and low water condensation rates, once the localized corrosion starts, its rate can be increased by the surface temperature.

The results of uniform TLC and maximum penetration rate, as a function of $p\text{CO}_2$ and condensation rate for the specimens after the TLC experiment at $p\text{CO}_2$ of 20 bar and 50 bar for solution temperature of 50 °C, are shown in Figure 20. As seen in Figure 20 (a), no clear dependency of the TLC rate on the $p\text{CO}_2$ is observed at this range. According to Figure 20 (b), under this experimental condition, the risk of localized corrosion exists for HWCR and LWCR specimens with no significant dependency on $p\text{CO}_2$ in this range. Interestingly, for the Gas phase specimens, the risk of localized corrosion is significantly reduced by increasing the $p\text{CO}_2$ from 20 to 50 bar. This decrease in the maximum penetration rate with $p\text{CO}_2$ for the Gas phase specimen could be due to the formation of a protective FeCO_3 layer that is favored by the increased $[\text{CO}_3^{2-}]$ content.

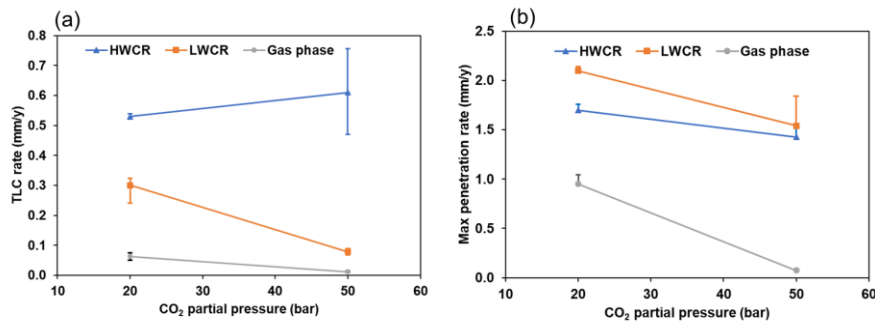


Figure 20: (a) uniform TLC and (b) maximum penetration rate as a function of $p\text{CO}_2$ and condensation rate (T_{sol} of 50 °C, duration of 21 days, error bars show max and min).

CONCLUSIONS

The following conclusions can be drawn from this study:

- Under the conditions of this study, no localized corrosion was detected during the first 7 days of the experiment for specimens exposed to different water condensation regimes. 21 days of exposure were necessary to expose localized corrosion.
- Uniform and localized TLC rate increased with the water condensation rate.
- The uniform and localized TLC rate increased with the surface temperature; however, this increase was more significant at higher water condensation rates.

- At different water condensation rates, the change in uniform and localized TLC rate with pCO₂ seemed insignificant.
- At the lowest water condensation rate tested, the formation of a protective FeCO₃ layer was favored at high pCO₂ which decreased the uniform and localized TLC rate.
- In the supercritical CO₂ environment, the difference in temperature between the CO₂ dense phase and the temperature of the specimen caused water drop-out and corrosion.
- In the supercritical CO₂ environment, the high CO₂ pressure and low pH of the dropped-out water led to high uniform and localized TLC rates.

ACKNOWLEDGEMENTS

Financial support from the following companies is greatly appreciated: PTTEP, Shell, and Saudi Aramco. Valuable technical support from Mr. Alexis Barxias and Mr. Cody Shafer is highly appreciated.

REFERENCES

1. J.R. Piccardino, P. Tanaprasertsong, Y. Gunaltun, M. Stuvik, "Internal Inspection of Wet Gas Lines Subject to Top of Line Corrosion," CORROSION/2004, paper no. 04354 (New Orleans, LA: NACE International, 2004).
2. Y.M. Gunaltun, D. Supriyatman, "Top of the Line Corrosion in Multiphase Gas Lines: A Case History," CORROSION/99, paper no. 99036, (San Antonio, TX: NACE International, 1999).
3. M. Singer, *Top-of-the-Line Corrosion*, 1st ed. A.M. El-Sherik, ed. (Boston: Woodhead Publishing, 2017), p. 385-408.
4. M. Singer, D. Hinkson, Z. Zhang, H. Wang, S. Nešić, "CO₂ Top-of-the-Line Corrosion in Presence of Acetic Acid: A Parametric Study," *Corrosion* 69, 7 (2013): p. 719-735.
5. D. Hinkson, Z. Zhang, M. Singer, S. Nešić, "Chemical Composition and Corrosiveness of the Condensate in Top-of-the-Line Corrosion," *Corrosion* 66, 4 (2010): p. 045002-045008.
6. M. Singer, J. Al-Khamis, S. Nešić, "Experimental Study of Sour Top-of-the-Line Corrosion Using a Novel Experimental Setup," *Corrosion* 69, 6 (2013): p. 624-638.
7. M. Singer, S. Nesic, Y. Gunaltun, "Top of the Line Corrosion in Presence of Acetic Acid and Carbon Dioxide," CORROSION 2004(NACE-04377: NACE International, 2004).
8. M.M. Islam, T. Pojtanabuntoeng, R. Gubner, "Condensation Corrosion of Carbon Steel at Low to Moderate Surface Temperature and Iron Carbonate Precipitation kinetics," *Corros. Sci.* 111, (2016): p. 139-150.
9. F. Vitse, S. Nešić, Y. Gunaltun, D.L. de Torreben, P. Duchet-Suchaux, "Mechanistic Model for the Prediction of Top-of-the-Line Corrosion Risk," *Corrosion* 59, 12 (2003): p. 1075-1084.
10. M. Singer, "Study and Modeling of the Localized Nature of Top of the Line Corrosion" (Ph.D. dissertation, Ohio University, 2013).
11. R. Nyborg, A. Dugstad, "Top of Line Corrosion and Water Condensation Rates in Wet Gas Pipelines," CORROSION/2007, paper no. 07555, (Nashville, TN: NACE International, 2007).
12. R.A. Ojifinni, C. Li, "A Parametric Study of Sweet Top-of-Line Corrosion in Wet Gas Pipelines," CORROSION/2011(NACE-11331: NACE International, 2011), p. paper no. 11331.
13. G. Svenningsen, M. Foss, R. Nyborg, H. Fukagawa, I. Kurniawan, "Top of Line Corrosion with High CO₂ and Organic Acid," CORROSION/2013, paper no. 2591, (Orlando, FL: NACE International, 2013).
14. T. Pojtanabuntoeng, M. Eslami, M. Singer, S. Nešić, "Influence of the Co-Condensation of Water and n-Heptane on Top of the Line Corrosion," *Corrosion* 78, 4 (2022): p. 295-306.
15. M. Eslami, M. Singer, "Study of Inhibition Efficiency of Model Volatile Corrosion Inhibitors in the Presence of N-Heptane," AMPP Annual Conference+ Expo/2022, paper no. 18003 (San Antonio, TX: AMPP, 2022).
16. J.Q. Wang, A. Atrens, D.R. Cousens, N. Kinaev, "Microstructure of X52 and X65 pipeline steels," *J. Mater. Sci.* 34, 8 (1999): p. 1721-1728.
17. B. Craig, "Should supercritical CO₂ pipelines comply with ANSI/NACE MR0175/ISO 15156?," *Mater. Perform.* 53, 12 (2014): p. 60-62.

18. ASTM G1-03, "Standard Practice for Preparing, Cleaning, and Evaluating Corrosion Test Specimens" (West Conshohocken, PA: ASTM International, 2011).
19. T.R. Andersen, A.M.K. Halvorsen, A. Valle, A. Dugstad, "The Influence of Condensation Rate and Acetic Acid Concentration on Tol-Corrosion in Multiphase Pipelines," CORROSION/2007, paper no. 07312, (Nashville, TN: NACE International, 2007).
20. C. Wang, L.a. Ren, J.B. Walters, L. Zhang, R. Tao, " In situ Raman vibrational spectra of siderite (FeCO_3) and rhodochrosite (MnCO_3) up to 47 GPa and 1100 K," *Am Min* 108, 2 (2023): p. 312-325.
21. S. Qian, Y.F. Cheng, " Corrosion of X52 steel under thin layers of water condensate in wet gas pipelines," *J. Nat. Gas Sci.* 68, (2019): p. 102921.
22. M.P.E. Ishmael, M.Z. Lukawski, J.W. Tester, " Isobaric heat capacity (C_p) measurements of supercritical fluids using flow calorimetry: equipment design and experimental validation with carbon dioxide, methanol, and carbon dioxide-methanol mixtures." *J. Supercrit. Fluids* 117, (2016): p. 72-79.
23. H. Qin, L. Xu, M. Lu, L. Zhang, W. Chang, "Top of the Line Corrosion under Low Temperature and High Condensation Rate Conditions," CORROSION/2011, paper no. 11328, (Houston, TX: 2011).